Fabrication and microstrain evolution of Al-TiB_2 composite coating by cold spray deposition

H. Chen[1,*], Z. Pala[2], T. Hussain[2] and D. G. McCartney[2]

[1]Department of Mechanical, Materials and Manufacturing Engineering, Faculty of Science and Engineering, University of Nottingham Ningbo China, Ningbo 315100, China

[2]Advanced Materials Research Group, Faculty of Engineering, University of Nottingham, University Park, Nottingham NG7 2RD, UK

Abstract

This paper investigates the microstructure evolution of Al-TiB_2 coatings prepared by cold spraying. In situ Al-TiB_2 composite powders containing uniformly distributed titanium diboride (TiB_2) particles with a size range of 5 to 100 nm in the Al matrix and Al/Al-TiB_2 blended powders were used as the cold spray feedstock for coating fabrication on aluminium alloy substrates. The microstructures of the feedstock powders and as-deposited coatings were characterised using scanning electron microscopy with energy dispersive X-ray (EDX) analysis and X-ray diffraction (XRD). Al/Al-TiB_2 blended powder coatings, compromising closely packed powder particles, were sprayed to an approximate thickness of 500 μm. Al-TiB_2 composite coatings (approximately 50 μm thick) were obtained retaining the microstructure of the composite powders being sprayed and no evidence of detrimental phase transformation was found. However, micro-cracks were found to exist in the Al-TiB_2 coating due to the hardly deformable powder particles. Little or no microstrain was revealed in the as-sprayed Al-TiB_2 coating, indicating that annealing may have occurred due to the localised adiabatic heating during the spraying process. It is demonstrated that it is possible to fabricate

the Al-TiB_2 composite coating by cold spray deposition but further improvements to eliminate coating cracking are required.

Keywords: Aluminium matrix composite; Cold spray; Al-TiB_2; Cracking; Microstrain

*Corresponding Author. Tel.: +86-574-88180946; Fax: +86-574-88187462.

E-mail address: Hao.Chen@nottingham.edu.cn

1. Introduction

Aluminium matrix composites (AMCs) have emerged as high performance structural materials for a wide range of applications in aerospace, automotive and transportation industries because of their improved strength, modulus and enhanced wear resistance compared to unreinforced bulk alloys.[1-3] Ceramic reinforced aluminium matrix composites is of particular interest due to their tribological, wear, creep and fatigue properties can be tailored to meet specific requirements by controlling the volume fraction, particle size and distribution of the reinforcing particles in the aluminium matrix.[4-7] Conventional ceramic particles, such as carbides, oxides, nitrides and borides, are widely used to reinforce aluminium alloys.[8-14] Among these reinforcements, more recently, titanium diboride (TiB_2) has been an attractive candidate since it exhibits high hardness and modulus.[15] The TiB_2 reinforced AMCs (Al-TiB_2) have been achieved by various manufacturing methods, e.g. friction stir processing[16-18], gas pressure infiltration[19, 20], in-situ reactive processes[21, 22], etc. Meanwhile, Al-TiB_2 composites are also employed as coatings to improve the wear resistance and hardness of aluminium and its alloys, especially in the structures where the properties of the surface layers are of primary importance. However, careful considerations are needed in coating production in order to maintain the original composite structure and to avoid any detrimental phase formation.

One method that appears to have the potential to meet the above requirements is the cold gas dynamic spraying or, more simply, cold spray. Unlike plasma spray and high velocity oxy-fuel thermal spray,[23-28] which use high temperature jets, cold spray involves the acceleration and impact of solid particles onto a substrate to form a coating at moderate to low temperatures. The bulk of the particles do not undergo any melting in cold spray; however, the temperature at the interfacial zone can rise significantly. Powder particles are accelerated by a supersonic gas jet to velocities in a range of 300 – 1200 m/s through a convergent-divergent de Laval nozzle.[29] Particles impinging on a substrate will either rebound or bond

with the substrate depending on the material type and, more importantly, particle velocity on impact with the substrate.[30] Bonding occurs at sufficient kinetic energy of the impinging particles, which allow rapid and significant deformation of the powder particles under high pressures and strain rates (10^{6-9} s^{-1}).[31] Compressive stress is usually developed in the cold sprayed coatings due to the relatively low temperatures and high strain induced during impact. Since the temperature is much below the melting point of the feedstock powder, oxidation, phase transformations as well as chemical decomposition of the powder can be inhibited. Thus the desirable properties of the powders are retained in cold sprayed coatings.[32]

Hitherto, cold spraying has been utilised to deposit many types of materials include pure metals, alloys and, more recently, composite materials. Examples include TiO_2-Zn[33], SnO_2-Ag[34], WC-Co[35], WC-Ni[36], Al_2O_3-Cu[37], Al_2O_3-Al[38], Al-SiC[39], Cr_3C_2-Ni[40], SiC-Al-Si[41], Al/Al-Si[42] and TiB_2-Cu[43]. In all the above cases of composite coatings, cold spraying has been demonstrated to be able to obtain uniformly distributed reinforcing phase within the matrix. However, studies of composite coatings such as Al-TiB_2 deposited by cold spraying does not appear to have been previously reported. It is generally recognised that spraying of ceramics is difficult because of its brittleness, it is challenging to study the behaviour of composite powders with high content of TiB_2. In addition, although it is commonly believed that large microstrains are generated in the coating since the cold spraying relies on plastic deformation for coating formation[44], it was noticed that the thermally activated recovery process could occur during cold spraying, especially in Al contained coatings, causing thermal softening rather than strain hardening.[45] But none of the above existing works on Al composite coatings have examined the microstrain development in cold sprayed coatings. Since mechanical properties of such coatings can be affected by the residual stress/strain; therefore, the aims of the present study are to elucidate the microstructures of Al-TiB_2 composite coatings formed in cold spraying and to investigate the microstrain evolution from the initial mechanically alloyed powder to the deposited coating.

2. Materials and experimental techniques

2.1. Materials

Al-20 wt.% TiB_2 powder having a particle size ~20 μm was obtained from a double-step mechanical alloying process (referred as Al-TiB_2 hereafter). The details of this process and procedures are given elsewhere.[21] Aluminium powder of 99.7% purity was obtained from Alpoco Ltd (Minworth, UK) and had a size range from 15 to 45 μm. Soft Al powder and hard, mechanically alloyed, Al-TiB_2 powder were mixed together in the required weight proportion (1:1) and blended in a turbula mixer for 2 h in air to obtain a blended powder. Subsequently the Al + 50 wt.% Al-TiB_2 blended powder and Al-TiB_2 powder were employed as feedstock materials for cold spraying. The above powders were deposited onto samples cut from AA6061 plate, sample dimensions were 75 × 25 × 3 mm^3. The aluminium alloy substrates were prepared by grit blasting with Al_2O_3 having a particle size ~500 μm under a nominal blasting pressure of 0.5 MPa and then degreased with alcohol prior to spray deposition. The coatings obtained by deposition of the Al-TiB_2 and blended Al-50 wt.% Al-TiB_2 powders and are designated as Al-TiB_2 coating and blended powder coating respectively.

2.2. Cold spraying

Cold spraying was carried out with an in-house built cold gas spraying system at the University of Nottingham comprising a high pressure gas supply, a high pressure powder feeder, a converging-diverging nozzle and an X-Y traverse unit. The detailed design of the cold spray system is described elsewhere.[46] Room temperature helium at 2.9 MPa was utilised as the process accelerating gas and nitrogen was employed as the powder carrier gas at a pressure of 3.0 MPa. The pressure difference between the carrier gas and the process gas is to facilitate powder transport into the main gas flow. A high pressure powder feeder (Praxair 1264HP, Indianapolis, IN, USA) with a powder feed wheel speed of 4 rpm (20 g/min) was used during the cold spraying process. The martensitic steel de Laval nozzle had a throat

diameter of 1.35 mm, with an area expansion ratio of ~8.8. The nozzle-substrate standoff distance for all the spray runs was fixed at 20 mm. The nozzle was attached to a frame and the substrates were fixed onto a computer controlled X-Y traverse table. Eight passes at a traverse speed of 100 mm·s^{-1} were used to build up the coating thickness for each feedstock powder. The velocity of particles for the chosen spraying parameters was 550-700 m/s depending on the size of the particles.

2.3. Microstructural characterisation

Powder samples were prepared by sprinkling a small quantity of loose powder onto an adhesive mount. Coating cross-sections were cut, mounted in a conductive resin and sequentially ground and diamond polished to a 1 μm surface finish. Prepared samples were examined in a FEI XL 30 scanning electron microscope (SEM) operated at 20 kV. Both secondary electrons (SE) and backscattered electrons (BSE) were used to form images and semi-quantitative energy dispersive X-ray analysis (EDX) was utilised for analysis of elemental compositions. Image analysis was carried out to measure coating porosity using the image analysis software Image J.[47] X-ray diffraction (XRD) of the powders and as-sprayed coatings was performed on a Bruker D-500 X-ray diffractometer operating at 40 kV and 25 mA using Cu-*K*α source with a wavelength of 0.15406 nm. XRD scans in the 2θ range 20° - 120° were conducted with a step size of 0.02° and 4 s counting time per step. Microstrain analysis was carried out using Williamson-Hall method[48] and whole powder pattern method (WPPM) incorporated in Rietveld refinement[49, 50]. The microhardness of coatings was measured on the polished coating cross-sections using a LECO M-400 microhardness tester with a 100 gf load and 15 s dwell time. Values quoted are the average of ten indents taken along the mid-plane of a coating cross-section.

3. Results

3.1. Powder Characteristics

Figure 1 shows the morphology of the blended powder and Al-TiB_2 powder. The blended powder shown in Figure 1(a) consists of spherical Al powder and irregular, rock shaped Al-TiB_2 powder varying from 5 to 25 μm. In the mechanically alloyed Al-TiB_2 powder, as shown in Figure 1(b), the larger particles are the Al matrix whilst the smaller satellites are the TiB_2 nanoparticles that exhibit a size range of 5 – 100 nm. Figure 2 shows the microstructure of a single Al-TiB_2 particle. EDX analysis revealed the darker phase to be the Al matrix, and the brighter phase to be the TiB_2 reinforcing particles. It is evident that the nanosized TiB_2 particles are distributed on the surface of the particle from Figure 2(a) and also embedded within the aluminium matrix from Figure 2(b). The XRD patterns of both powders shown in Figure 3 confirm that only two phases are present, aluminium and titanium diboride. No evidence for the minor phases such as TiAl and Al_3Ti intermetallic compounds can be found. It can be seen that the peaks associated with TiB_2 in the blended powder are not as intensive as those in the Al-TiB_2 powder, which is due to the lower content of TiB_2 in the blended powder.

3.2. Microstructure of coatings

The microstructures of the cold sprayed blend powder coatings and Al-TiB_2 coatings are shown in Figure 4. It is seen that the blended powder resulted in a much thicker coating, ~500 μm, and the thickness of the Al-TiB_2 coating was only ~50 μm. The blended powder coating shown in Figure 4(a) and (b) is composed of a uniformly distributed mixture of Al and Al-TiB_2 powder particles. The two phase microstructure and the shape of the Al-TiB_2 particles in the blended powder coating was retained, consisting of the light contrast TiB_2 particles and the dark contrast Al matrix. The blended powder coating has a porosity less than 2% from image analysis in Figure 4(a) but poor interface bonding between the Al-TiB_2 and the Al particles is found in Figure 4(b). Micron sized cracks are visible in the Al-TiB_2 coating as

shown in Figure 4(c) and (d). These tend to occur as delaminating cracks between the layers that have been deposited due to poor bonding resulted from poor particle deformation. Table 1 tabulates various processing and microstructural measurements for the coatings. It can be seen that the coatings have low porosity, less than 2% in both cases. A microhardness difference is also evident as shown in Table 1. The composite Al-TiB_2 coating exhibits higher hardness (132±22 HV) than the blended powder coating (71±15 HV). XRD patterns of as-sprayed coatings in Figure 5 confirm no evidence of new phase transformation during spraying.

3.3. Microstrain analysis

In order to investigate the evolution of microstrain and crystallite size in the Al matrix from the mechanically alloyed Al-TiB_2 composite powder to the as-sprayed Al-TiB_2 coating, the Williamson-Hall (WH) plot[48] and whole powder pattern method (WPPM) incorporated in Rietveld refinement[49, 50] were conducted. For the WH method,

$$\sqrt{B_M^2 - B_I^2}cos\theta = 4\varepsilon\, sin\theta + \frac{0.9\lambda}{D} \qquad (1)$$

where B_M is the measured full width half maximum (FWHM) from the original Al-TiB_2 powder and as-sprayed Al-TiB_2 coatings, B_I is the instrumental broadening from the well-annealed Al powder, θ is the diffraction angle, ε is the microstrain, λ is the wavelength of the X-rays used in nanometers (0.154056 nm for Cu-*K*α source) and D is the average crystallite size. The annealing of the Al powder was carried out at 350 °C in Argon for 8 h followed by furnace cooling. The WH plot is shown in Figure 6, demonstrating the microstrain embedded in the as-received Al-TiB_2 powder due to mechanical alloying. However, the slope of the as-sprayed Al-TiB_2 coating is almost zero, which indicates that little or no microstrain presents in the coating. The accuracy of the WPPM results is documented by very good correspondence between measured data and obtained fit in Figure 7. The average crystallite size and microstrain in the Al-TiB_2 powder and coating obtained are summarised in Table 2. The results obtained from WH plot matches very well with the WPPM results even though

only five aluminium reflections were used for WH plot and the whole powder XRD pattern for the WPPM analysis.

4. Discussion

4.1. Bonding mechanism

The less porous and almost crack-free structure of the blended powder coating, seen in Figure 4 (a) and (b) can be attributed to the high deposition efficiency of readily deformable Al powder. As has been previously reported by Bakshi et al.,[42] the pure Al powder can be sprayed to a much thicker coating compared to the Al powder mixtures, i.e. Al/Al-Si. It is possible that the soft Al powders entrap the Al-TiB_2 powder particles between the deforming Al particles. Bonding occurred due to the extensive deformation of pure Al powder in the blended powder coating. Indeed Figure 4(a) and (b) provide the evidence that the Al-TiB_2 particles are entrapped by the pure Al powder in the blended coating. Meanwhile, poor bonding may exist at localised areas where the Al-TiB_2 particles were subjected to high impact forces, i.e. the brittle Al-TiB_2 initially bombarded the substrate, causing cracking of the Al-TiB_2 particles, as shown in Figure 4(b). The lower deformability of the Al-TiB_2 particles can lead to larger energy transfer to Al particles during impact. Since Al particles are relatively soft and easily deformable, splats can be built up to produce thick coating and high deposition efficiency was achieved.

The much thinner Al-TiB_2 coating indicates the lower deposition efficiency of Al-TiB_2 particles as compared to that of blended powder for the same spraying conditions and almost identical powder feed rates. The deformation of particles is largely due to the deformation of soft Al matrix in the composite particles. The nanosized and hardly deformable TiB_2 is widely retained and extensive cracking occurred in the Al-TiB_2 coating. Since the bonding typically relies on the deformation of the particles in the cold spraying, the high content of TiB_2 particles in the powder experiences little or no deformation. The splats cannot be deformed as

much as that in the blended powder coating and they either rebound or spall off from the pre-deposited layers, causing a thinner coating with extensive cracks as seen in Figure 4(c) and (d). Critical particle velocities of most metals and alloys for cold spray deposition were reported to be in the range of 500 – 700 m/s by theoretical calculation and experimental works.[51] It can be generally summarised into the following equation,

$$V_{critical}\,(m/s) = 667 - 14\rho + 0.08T_m + 0.1\sigma_u - 0.4T_i \qquad (2)$$

where ρ is the density in g/cm^3, T_m is the melting temperature in °C, σ_u is the ultimate strength in MPa, and T_i is the initial particle temperature in °C. The above equation is reasonable in the sense that the particle strengthening will increase the critical particle velocity because as the strength is increased, less deformation of the particle would occur. As a result, the critical velocity will be increased to allow enough deformation of the strengthened particles to assist the bonding between the sprayed particles. Since it is already known that materials properties can have substantial influences on the critical velocity in cold spraying, Schmidt et al.[52] worked to improve the accuracy of Eq. (2), in which the mechanical balance of an impact is proposed, as simplified in Eq. (3),

$$V_{critical}\,(m/s) \sim \sqrt{\sigma_{TS}} \qquad (3)$$

where σ_{TS} is the tensile strength. With experimentally measured hardness values of spray powders, the tensile strength can be replaced by the Vickers hardness to estimate the critical velocity. Taking the hardness value from Table 1, it is found that,

$$V_{critical}\,(Al - TiB_2) \sim 1.8\,V_{critical}\,(Al) \qquad (4)$$

The critical velocity for aluminium powder with particle size below 45 μm was determined to be approximately 660-700 m/s.[51] Since the velocity of particles used was 550-700 m/s for cold spraying in this study, it can be concluded from Eq. (4) that the impact velocities for Al-TiB_2 powders were insufficient to produce good particle deformation and intimate particle/particle bonding, leaving cracks at the interlamellar region.

4.2. Microstrain interpretation

It is well known that the mechanical alloying generates the internal strain in the crystal lattice due to the high speed in situ ball milling process. This internal strain usually causes the peak broadening in the X-ray diffraction analysis, as seen from Figure 3 where Al peak in the Al-TiB_2 powder are slightly broader. It is widely believed that the cold spraying involves plastic deformation of powder particles with large resultant strain (100%~300%).[45] However, this was not observed and on the contrary, the Al peaks became narrower and no clear microstrain was found in the Al-TiB_2 coating. This may be attributed to the localised heat generated at the particle interface, which acted as an annealing effect to remove the microstrain of the coating. During the cold spraying process, the initial kinetic energy of the in-flight particle is mainly dissipated into plastic deformation and viscous effects/frictional work of the impacting particle and substrate, provided that the coatings were deposited well by cold spraying. But in this study, since the soft Al matrix is reinforced by the non-deformable TiB_2 particles, less deformation occurred during cold spraying. The low deposition efficiency indicates that the mechanically alloyed composite powders were not sprayed well and most of them rebounded due to their poor deformability. This can be treated as the shot peening process in which the kinetic energy of in-flight particles has mainly been transferred to the heat to the pre-deposited layers. The heat generated may be conducted away or fluxed out, to justify the adiabatic heating, using the similar approach proposed by Assadi et al.,[51]

$$x_d = \sqrt{D_{th} \cdot t_{impact}} \qquad (5)$$

where x_d is the heat diffusion distance, D_{th} is the thermal diffusivity, taken as 8.5×10^{-5} m^2/s and t_{impact} is the total impact time. x_d is found around 47 μm, which is close to the Al-TiB_2 coating thickness of ~50 μm. Therefore, the adiabatic heating condition applies, indicating that the continuous impact particles through cold spraying caused the heat accumulation in the coating. This gives an instant temperature increase of approximately 220~260 °C during impact, which agrees well with the reported work that the average temperature of Al under

impact conditions during cold spray can achieve 44% or even higher of the Al melting temperature.[45] Consequently, the annealing of the coating occurred and microstrain in the coating diminished. The growth in the crystalline size of Al matrix from Table 2 further supports this view. It should be noted that the heat generated did not lead to any oxidation since oxide peaks were not found in the Al-TiB_2 coating in Figure 5. Even with little or no microstrain in the Al-TiB_2 coating, it still exhibits a higher hardness compared to the blended powder coating, which is attributed to the fact that the higher volume fraction of the TiB_2 particles in the Al-TiB_2 coating.

4.3. Comparison with previous studies

Composite powders have been successfully cold sprayed in a few studies. Generally, cold sprayed composite coatings, depending on the spray parameters used, are about 50-100 μm due to the presence of hardly deformable reinforcing phase. It is also quite common that the composite structure of the feedstock powder is typically retained. Cracks also exist in other similar studies and low deposition efficiencies were reported when cold spraying of composite powders.[43] It has been shown that the porosity resulted from cold spraying of Al and Al/Al-Si systems with almost identical spraying parameters is generally below 2%, which agrees well with the porosity that obtained in this study.[42] Much lower deposition efficiency of Al-TiB_2 powder was found in the present study compared to the blended powder as seen in Figure 4, which is consistent with the work reported previously.[42] But none of the previous studies have focused on the microstrain evolution on cold spraying composite powders. Ajdelsztajn et al.[53] suggested that the heat may be generated during the continuous impact of rebounded particles during cold spraying and thermal softening would occur. Such phenomenon could be consistent with the little or no microstrain in this cold sprayed Al-TiB_2 coating. However, due to the spraying parameters vary among the reported work and it is hard to make direct comparison with other studies. Although it is clear that further work is needed

with cold spraying to establish with better control of spraying parameters for this Al-TiB_2 composite powders, it is evident that the Al-TiB_2 composite powders can be successfully deposited by cold spraying to form composite coatings. Further work is necessary to carefully manipulate the spraying parameters and conditions to produce crack-free Al-TiB_2 coatings by cold spraying.

5. Conclusions

- Two different coatings were prepared by cold spraying, namely the blended powder coating and Al-TiB_2 coating, no new phase formation was observed after spraying. The blended powder coating was thick and less porous while the Al-TiB_2 coating was thin with cracks. The soft Al powder entraps the hard Al-TiB_2 powder in the blended powder to facilitate the coating formation.
- The low deposition efficiency of Al-TiB_2 coating was attributed to the high volume fraction of hard and non-deformable Al-TiB_2 particles. Micro-cracks were found in the Al-TiB_2 coating, which is possibly due to the poor bonding of Al-TiB_2 particles, leading to the cracks at the interlamellar region.
- Little or no microstrain was found in the Al-TiB_2 coating compared to that in the initial mechanically alloyed Al-TiB_2 powder. This is due to the heat generated during spraying that acted as an annealing effect, as such the microstrain in the coating was relieved. Further work is necessary to eliminate the cracks by carefully controlling the cold spraying parameters.

6. Acknowledgements

The authors would like to acknowledge Faculty of Engineering, University of Nottingham for provision of laboratory facilities. The financial support from Nature Science Foundation of China (No. 21403119), Zhejiang Natural Science Foundation Programme (No.

LQ16E060001), Zhejiang Commonweal Technology Project (No. 2016C31023), Ningbo Enrich People Project (2016C10035) and Ningbo Natural Science Foundation Programme (No. 2016A610114) are acknowledged.

7. Declaration of Conflicting Interests

The author(s) declared no potential conflicts of interest with respect to the research, authorship, and/or publication of this article.

8. Funding

This research received no specific grant from any funding agency in the public, commercial, or not-for-profit sectors.

9. References

1. Miracle DB. Metal matrix composites – From science to technological significance. *Compos Sci Technol*. 2005; 65: 2526-2540.
2. Dlouhy A, Merk N and Eggeler G. A microstructural study of creep in short fibre reinforced aluminium alloys. *Acta Metall Mater*. 1993; 41: 3245-3256.
3. Cantor B, Dunne F and Stone I. *Metal and Ceramic Matrix Composites*. London: IOP Publishing, 2004.
4. Kaczmar JW, Pietrzak K and Włosiński W. The production and application of metal matrix composite materials. *J Mater Process Technol*. 2000; 106: 58-67.
5. Harrigan Jr WC. Commercial processing of metal matrix composites. *Mater Sci Eng A*. 1998; 244: 75-79.
6. Ralph B, Yuen HC and Lee WB. The processing of metal matrix composites — an overview. *J Mater Process Technol*. 1997; 63: 339-353.
7. Zhang Q, Zhang W, Liu Y and Guo B. Cyclic compressive creep-elastoplastic behaviors of in situ TiB_2/Al-reinforced composite. *Mater Sci Eng A*. 2016; 666: 1-9.
8. Shafiei-Zarghani A, Kashani-Bozorg SF and Hanzaki AZ. Wear assessment of Al/Al_2O_3 nano-composite surface layer produced using friction stir processing. *Wear*. 2011; 270: 403-412.
9. Dolatkhah A, Golbabaei P, Besharati Givi MK and Molaiekiya F. Investigating effects of process parameters on microstructural and mechanical properties of Al5052/SiC metal matrix composite fabricated via friction stir processing. *Mater Des*. 2012; 37: 458-464.
10. Chang F, Gu D, Dai D and Yuan P. Selective laser melting of in-situ Al4SiC4 + SiC hybrid reinforced Al matrix composites: Influence of starting SiC particle size. *Surf Coat Technol*. 2015; 272: 15-24.
11. Yuan P, Gu D and Dai D. Particulate migration behavior and its mechanism during selective laser melting of TiC reinforced Al matrix nanocomposites. *Mater Des*. 2015; 82: 46-55.

12. Ma SM, Zhang P, Ji G, Chen Z, Sun GA, Zhong SY, Ji V and Wang HW. Microstructure and mechanical properties of friction stir processed Al–Mg–Si alloys dispersion-strengthened by nanosized TiB_2 particles. *J Alloys Compd*. 2014; 616: 128-136.
13. Zhang Y, Ma N and Wang H. Effect of particulate/Al interface on the damping behavior of in situ TiB_2 reinforced aluminium composite. *Mater Lett*. 2007; 61: 3273-3275.
14. Pialago EJT, Kwon OK, Kim M-S and Park CW. Ternary Cu–CNT–AlN composite coatings consolidated by cold spray deposition of mechanically alloyed powders. *J Alloys Compd*. 2015; 650: 199-209.
15. Basu B, Raju GB and Suri AK. Processing and properties of monolithic TiB_2 based materials. *Int Mater Rev*. 2006; 51: 352-374.
16. Narimani M, Lotfi B and Sadeghian Z. Evaluation of the microstructure and wear behaviour of AA6063-B_4C/TiB_2 mono and hybrid composite layers produced by friction stir processing. *Surf Coat Technol*. 2016; 285: 1-10.
17. Chen Z, Li J, Borbely A, Ji G, Zhong SY, Wu Y, Wang ML and Wang HW. The effects of nanosized particles on microstructural evolution of an in-situ TiB_2/6063Al composite produced by friction stir processing. *Mater Des*. 2015; 88: 999-1007.
18. Rajan HBM, Dinaharan I, Ramabalan S and Akinlabi ET. Influence of friction stir processing on microstructure and properties of AA7075/TiB_2 in situ composite. *J Alloys Compd*. 2016; 657: 250-260.
19. Molina JM, Tian J, Narciso J and Louis E. Fabrication of Al/TiB_2 composites through gas pressure infiltration. *J Mater Sci*. 2010; 45: 2816-2821.
20. Karbalaei Akbari M, Baharvandi HR and Shirvanimoghaddam K. Tensile and fracture behavior of nano/micro TiB_2 particle reinforced casting A356 aluminum alloy composites. *Mater Des*. 2015; 66A: 150-161.
21. Sadeghian Z, Enayati MH and Beiss P. In situ production of Al–TiB_2 nanocomposite by double-step mechanical alloying. *J Mater Sci*. 2009; 44: 2566-2572.
22. Lü L, Lai MO, Su Y, Teo HL and Feng CF. In situ TiB_2 reinforced Al alloy composites. *Scripta Mater*. 2001; 45: 1017-1023.
23. Chen H and Hyde TH. Use of multi-step loading small punch test to investigate the ductile-to-brittle transition behaviour of a thermally sprayed CoNiCrAlY coating. *Mater Sci Eng A*. 2017; 680: 203-209.
24. Chen H, Hyde TH, Voisey KT and McCartney DG. Application of small punch creep testing to a thermally sprayed CoNiCrAlY bond coat. *Mater Sci Eng A*. 2013; 585: 205-213.
25. Chen H, McCartney DG and Voisey KT. Effect of surface conditions on internal oxidation and nitridation of HVOF MCrAlY coatings. *Mater High Temp*. 2015; 32: 215-220.
26. Chen H, Hyde TH, Voisey KT and McCartney DG. Effects of pre-cracking on small punch creep testing of a vacuum plasma-sprayed CoNiCrAlY coating. *Proc IMechE Part L: J Materials: Design and Application*. 2016.
27. Chen H, Jackson GA, Voisey KT and McCartney DG. Modelling and experimental study on β-phase depletion behaviour of HVOF sprayed free-standing CoNiCrAlY coatings during oxidation. *Surf Coat Technol*. 2016; 291: 34-42.
28. Chen H, Yang J and Xiao XL. Evaluation of the ductile-to-brittle transition temperature in a thermally sprayed CoNiCrAlY coating by small punch multi-step loading tests. *Proc IMechE Part L: J Materials: Design and Application*. 2016.
29. Grigoriev S, Okunkova A, Sova A, Bertrand P and Smurov I. Cold spraying: From process fundamentals towards advanced applications. *Surf Coat Technol*. 2015; 268: 77-84.
30. Luo X-T, Li C-X, Shang F-L, Yang G-J, Wang Y-Y and Li C-J. High velocity impact induced microstructure evolution during deposition of cold spray coatings: A review. *Surf Coat Technol*. 2014; 254: 11-20.
31. Hussain T, McCartney DG, Shipway PH and Zhang D. Bonding Mechanisms in Cold Spraying: The Contributions of Metallurgical and Mechanical Components. *J Therm Spray Technol*. 2009; 18: 364-379.

32. Villafuerte J. *Modern Cold Spray*. Switzerland: Springer International Publishing, 2015.
33. Morimoto J, Onoda T, Sasaki Y and Abe N. Improvement of solid cold sprayed TiO_2–Zn coating with direct diode laser. *Vacuum*. 2004; 73: 527-532.
34. Wang J, Zhou X, Lu L, Li D, Mohanty P and Wang Y. Microstructure and properties of Ag/SnO_2 coatings prepared by cold spraying. *Surf Coat Technol*. 2013; 236: 224-229.
35. Kim H-J, Lee C-H and Hwang S-Y. Fabrication of WC–Co coatings by cold spray deposition. *Surf Coat Technol*. 2005; 191: 335-340.
36. Lioma D, Sacks N and Botef I. Cold gas dynamic spraying of WC–Ni cemented carbide coatings. *Int J Refract Met Hard Mater*. 2015; 49: 365-373.
37. Triantou KI, Pantelis DI, Guipont V and Jeandin M. Microstructure and tribological behavior of copper and composite copper+alumina cold sprayed coatings for various alumina contents. *Wear*. 2015; 336–337: 96-107.
38. Wang Q, Birbilis N, Huang H and Zhang M-X. Microstructure characterization and nanomechanics of cold-sprayed pure Al and Al-Al_2O_3 composite coatings. *Surf Coat Technol*. 2013; 232: 216-223.
39. Wang Y, Normand B, Mary N, Yu M and Liao H. Microstructure and corrosion behavior of cold sprayed SiCp/Al 5056 composite coatings. *Surf Coat Technol*. 2014; 251: 264-275.
40. Cavaliere P, Perrone A and Silvello A. Mechanical and microstructural behavior of nanocomposites produced via cold spray. *Composites Part B*. 2014; 67: 326-331.
41. Li W, Chen ZH, Chen D, Teng J and Fan C. Low-cycle fatigue behavior of SiCp/Al–Si composites produced by spray deposition. *Mater Sci Eng A*. 2010; 527: 7631-7637.
42. Bakshi SR, Wang D, Price T, Zhang D, Keshri AK, Chen Y, McCartney DG, Shipway PH and Agarwal A. Microstructure and wear properties of aluminum/aluminum–silicon composite coatings prepared by cold spraying. *Surf Coat Technol*. 2009; 204: 503-510.
43. Kim JS, Kwon YS, Lomovsky OI, Dudina DV, Kosarev VF, Klinkov SV, Kwon DH and Smurov I. Cold spraying of in situ produced TiB_2–Cu nanocomposite powders. *Compos Sci Technol*. 2007; 67: 2292-2296.
44. Aldwell B, Yin S, McDonnell KA, Trimble D, Hussain T and Lupoi R. A novel method for metal–diamond composite coating deposition with cold spray and formation mechanism. *Scripta Mater*. 2016; 115: 10-13.
45. Luzin V, Spencer K and Zhang MX. Residual stress and thermo-mechanical properties of cold spray metal coatings. *Acta Mater*. 2011; 59: 1259-1270.
46. Zhang D, Shipway PH and McCartney DG. Cold gas dynamic spraying of aluminum: The role of substrate characteristics in deposit formation. *J Therm Spray Technol*. 2005; 14: 109-116.
47. Schneider CA, Rasband WS and Eliceiri KW. NIH Image to ImageJ: 25 years of image analysis. *Nat Methods*. 2012; 9: 671-675.
48. Williamson GK and Hall WH. X-ray line broadening from filed aluminium and wolfram. *Acta Metall*. 1953; 1: 22-31.
49. Rietveld H. A profile refinement method for nuclear and magnetic structures. *J Appl Crystallogr*. 1969; 2: 65-71.
50. Lutterotti L and Scardi P. Simultaneous structure and size–strain refinement by the Rietveld method. *J Appl Crystallogr*. 1990; 23: 246-252.
51. Assadi H, Gärtner F, Stoltenhoff T and Kreye H. Bonding mechanism in cold gas spraying. *Acta Mater*. 2003; 51: 4379-4394.
52. Schmidt T, Gärtner F, Assadi H and Kreye H. Development of a generalized parameter window for cold spray deposition. *Acta Mater*. 2006; 54: 729-742.
53. Ajdelsztajn L, Schoenung JM, Jodoin B and Kim GE. Cold spray deposition of nanocrystalline aluminum alloys. *Metall Mater Trans A*. 2005; 36: 657-666.

Tables

Table 1 Microstructural parameters and microhardness of the cold sprayed coatings.

Sample name	wt.% of Al-TiB_2 in the powder mixture	Vol.% of Al-TiB_2 particles	Vol.% of porosity	Coating thickness, µm	Vickers hardness, HV
Blended powder coating	50	37 ± 3	1.8 ± 0.4	500	71 ± 15
Al-TiB_2 coating	100	100	0.6 ± 0.3	50	132 ± 22

Table 2 Average crystalline size and lattice strain of Al matrix in the Al-TiB_2 powder and coating calculated by the Williamson-Hall (WH) plot and whole powder pattern method (WPPM).

Sample	Crystalline size (nm)		Lattice strain (%)	
	WH	WPPM	WH	WPPM
Al-TiB_2 powder	54	54	0.147	0.125
Al-TiB_2 coating	69	58	0	0

Figures

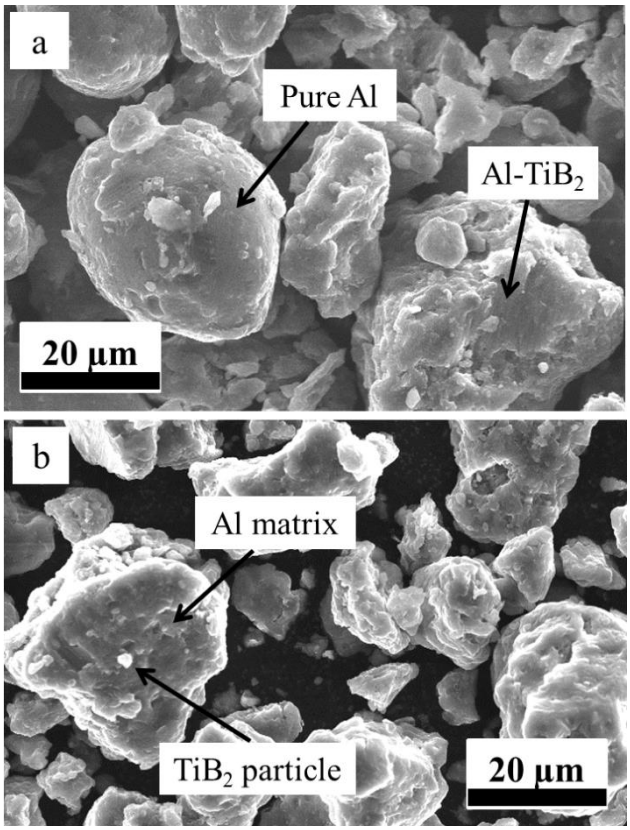

Fig. 1. Secondary electron SEM micrographs showing the morphology of 1:1 mixture of Al and Al-TiB_2 blended powder (a) and Al-TiB_2 powder (b).

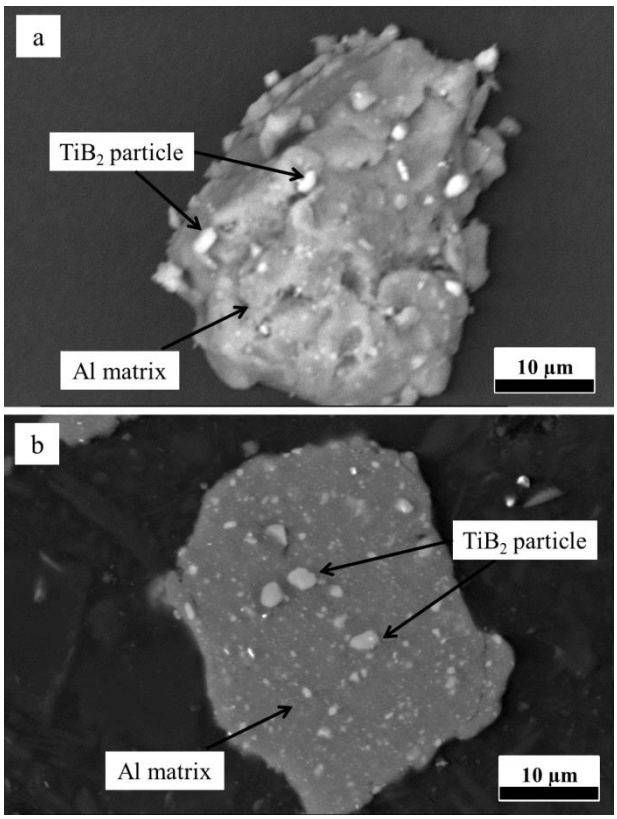

Fig. 2. Backscatter electron SEM micrographs showing the microstructure of the Al-TiB_2 powder particle: (a) overall structure and (b) cross section of the particle.

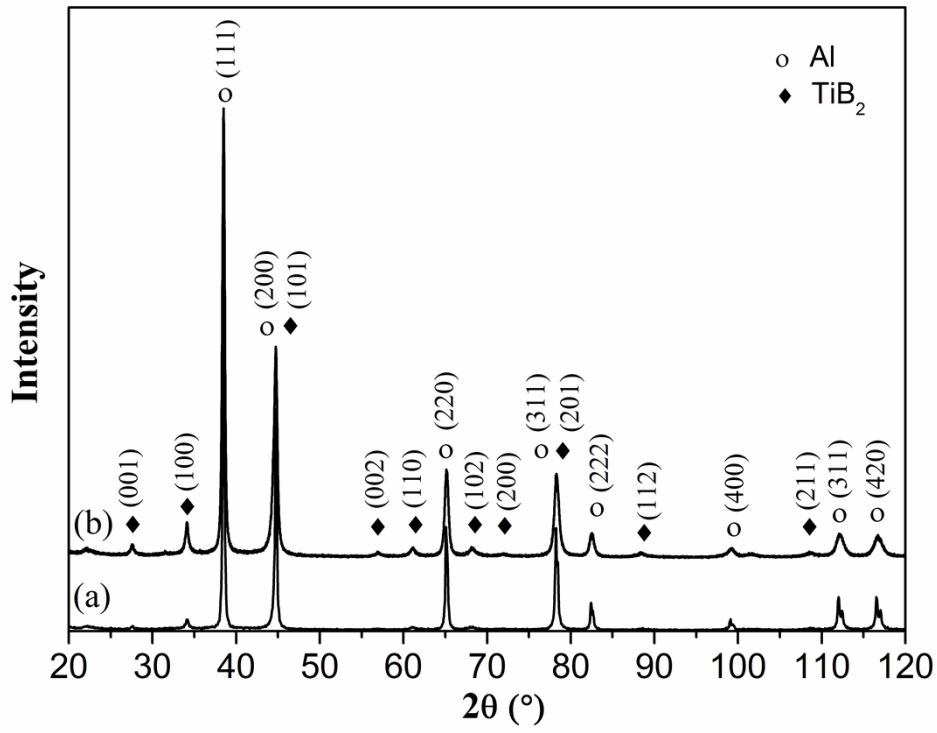

Fig. 3. XRD patterns of blended powder (a) and Al-TiB_2 powder (b).

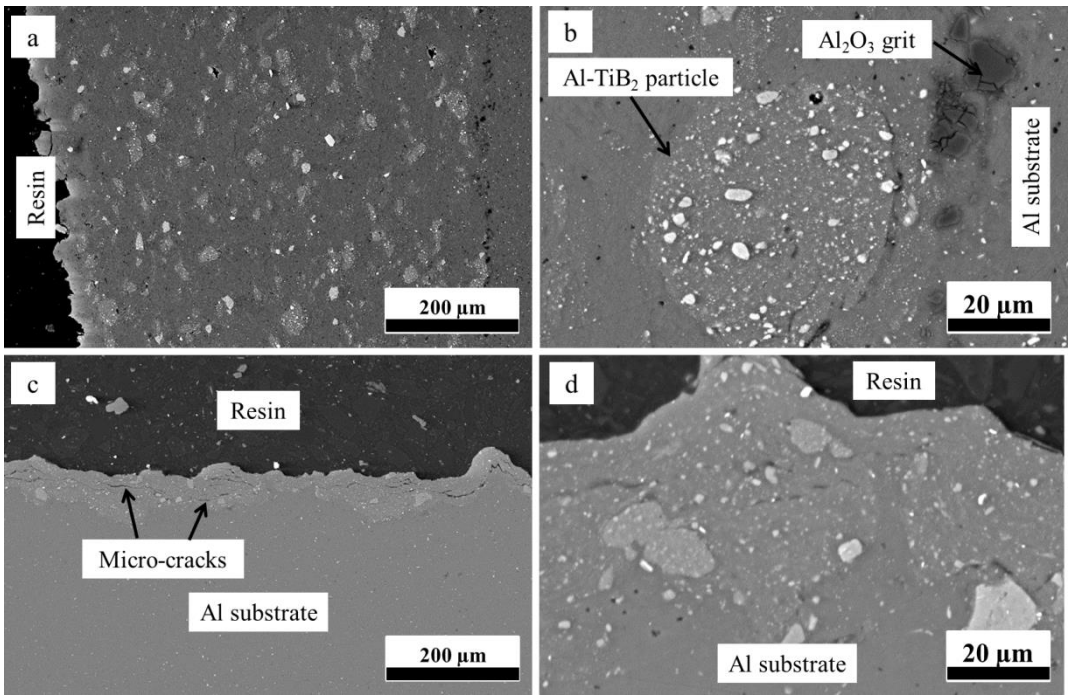

Fig. 4. SEM micrographs of the cross section of the cold sprayed coatings: (a) and (b) blended powder coating at low and high magnification; (c) and (d) Al-TiB_2 coating at low and high magnification.

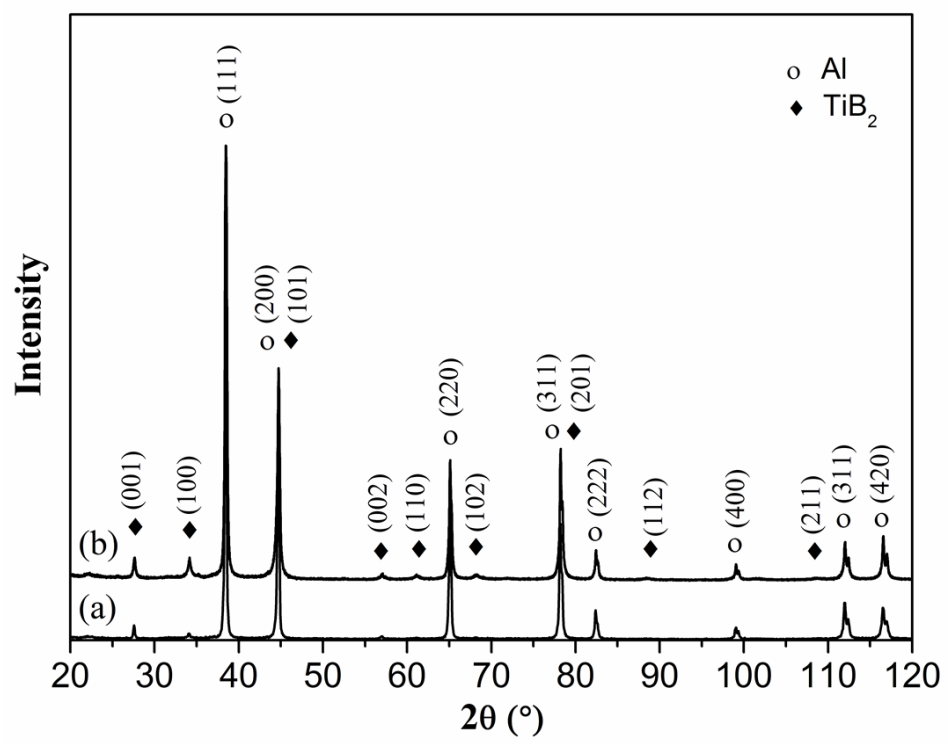

Fig. 5. XRD patterns of blended powder coating (a) and Al-TiB_2 coating (b).

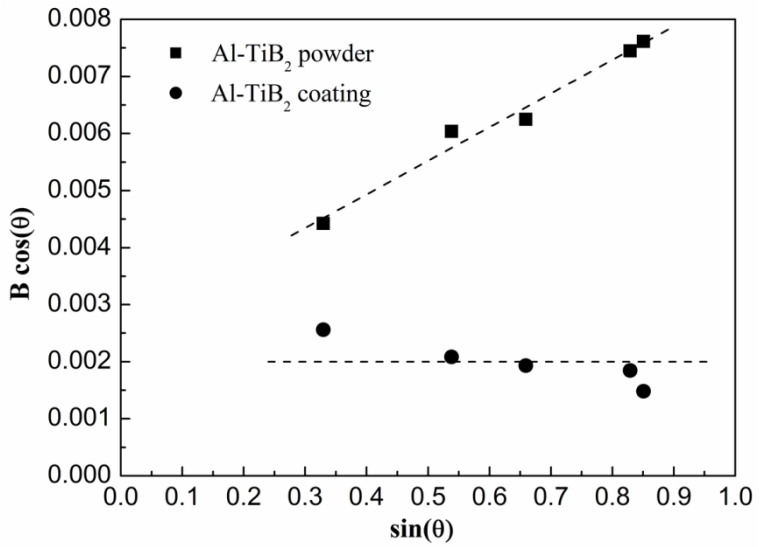

Fig. 6. Williamson-Hall plot of Al-TiB_2 powder and coating for microstrain analysis.

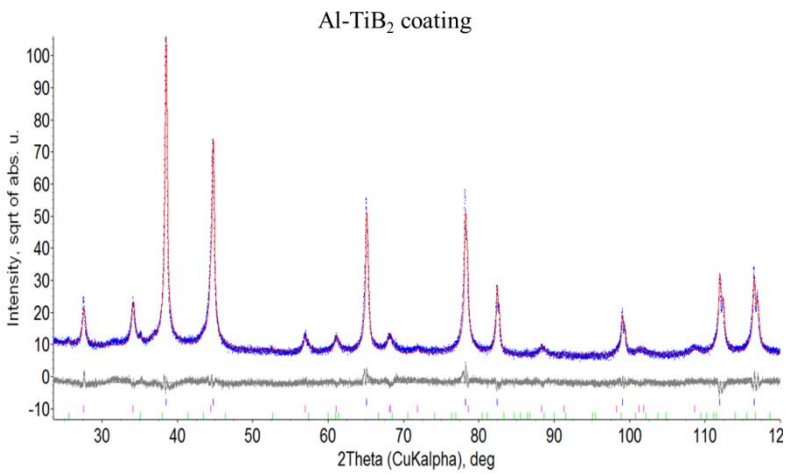

Fig. 7. Result of Rietveld refinement of Al-TiB_2 coating with WPPM incorporated for size-strain determination; blue points are measured data, red pattern is the obtained fit and gray curve at zero intensity is the difference curve.